Applied Catalysis B: Environmental 242 (2019) 31–39

Contents lists available at ScienceDirect

Applied Catalysis B: Environmental

journal homepage: www.elsevier.com/locate/apcatb

NiMo-ceria-zirconia-based anode for solid oxide fuel cells operating on gasoline surrogate

Xiaoxue Hou[a,1], Kai Zhao[a,b,1], Olga A. Marina[c], M. Grant Norton[a,d,*], Su Ha[a,*]

[a] Voiland School of Chemical Engineering and Bioengineering, Washington State University, Pullman, WA, 99164, USA
[b] School of Materials Science and Energy Engineering, Foshan University, Foshan 528000, People's Republic of China
[c] Energy Efficiency Division, Pacific Northwest National Laboratory, Richland, WA, 99352, USA
[d] School of Mechanical and Materials Engineering, Washington State University, Pullman, WA, 99164, USA

ARTICLE INFO

Keywords:
NiMo-ceria-zirconia composite
Single multifunctional anode layer
Solid oxide fuel cell
Internal reforming
Isooctane

ABSTRACT

A multi-functional NiMo-ceria-zirconia composite was developed as an anode for a solid oxide fuel cell (SOFC) running on isooctane, a commonly used gasoline surrogate. The anode layer was fabricated on an electrolyte-supported single cell using yttria-stabilized zirconia (YSZ) as the electrolyte and $La_{0.6}Sr_{0.4}Co_{0.2}Fe_{0.8}O_{3-\delta}$ as the cathode. Our results indicate that the single NiMo-ceria-zirconia layer possesses a dual-functionality: firstly to internally convert complex hydrocarbons into synthesis gas with a high resistance to coking and secondly to electrochemically oxidize the synthesis gas mixture for electric power generation. Compared with the conventional Ni-YSZ anode single cell, the application of the ceria-zirconia in the anode significantly suppresses carbon deposition and improves the performance stability of the single cell. Furthermore, the addition of Mo in the Ni-ceria-zirconia appears to facilitate a higher degree of sintering for the anode, which increases the electronic conductivity and maximum power density of the single cell. Consequently, at 800 °C the single cell with 5 wt.% Mo in the Ni-ceria-zirconia-based anode displayed a higher maximum power density of 212 mW cm^{-2} at 0.48 V and significantly enhanced performance stability than the conventional Ni-YSZ anode single cell in the isooctane/air operating mode.

1. Introduction

Solid oxide fuel cells (SOFCs) are highly efficient electrochemical devices that convert the chemical energy of fuels directly into electricity. Typically, SOFCs operate in the temperature range 600–1000 °C [1]. The high operation temperature offers the capability for direct utilization of complex liquid hydrocarbon fuels (e.g., gasoline, diesel-like fuels and kerosene-based jet fuels) and next generation liquid biofuels (e.g., biodiesel). By designing a suitable internal reforming unit, the complex liquid hydrocarbon fuels can be converted into a simple synthesis gas (a mixture of H_2 and CO) for electric power generation [2–4]. Although the internal reforming of complex liquid hydrocarbons could reduce the efficiency of an overall SOFC system, the net efficiency (e.g., 55%–60% for an isooctane/air fed SOFC) is still competitive when compared with a conventional gasoline internal combustion engine (~20%) or a gas turbine engine (~30%) [5–7].

Nickel-containing anodes, such as Ni-yttria-stabilized-zirconia (YSZ) and Ni-samaria-doped ceria (SDC) are commonly used in SOFCs due to their high mixed electronic-ionic conductivity, good electrochemical activity for electrochemical oxidation, and reasonable chemical compatibility with other fuel cell components [8–10]. However, nickel is a well-known catalyst for hydrocarbon cracking reactions, which could lead to severe surface carbon deposition in complex hydrocarbon fuels. Excessive formation of carbon deposits could block electrochemically active sites for fuel oxidation and inhibit gas diffusion in the anode [11,12]. These phenomena would increase electrode polarization, limit the electrochemical performance, and destroy the anode structure.

To address the stability issue in a coking environment, the nickel in the anode has been alloyed with other metals, such as Sn, Sb, Fe, Co, and Cu [13–21]. For example, binary alloys of NiSn and NiSb were suggested to remain stable in dry hydrocarbons [13,21]. Additionally, Cu is known to be less active toward the cracking of hydrocarbons. As a result, NiCu-containing anodes have been the subject of several investigations. First-principle density functional theory (DFT) calculations indicate that the barrier energy for successive hydrocarbon dehydrogenation is increased by embedding Cu into the Ni phase, which

* Corresponding authors at: Voiland School of Chemical Engineering and Bioengineering, Washington State University, Pullman, WA, 99164, USA.
E-mail addresses: mg_norton@wsu.edu (M. Grant Norton), suha@wsu.edu (S. Ha).
[1] These authors have contributed equally.

https://doi.org/10.1016/j.apcatb.2018.09.095
Received 10 April 2018; Received in revised form 26 September 2018; Accepted 30 September 2018
Available online 01 October 2018
0926-3373/ Published by Elsevier B.V.

destabilizes the adsorption of carbon on the nickel surface [22]. The DFT results have been verified experimentally. For example, the single cell employing a $Ni_{0.8}Cu_{0.2}$-SDC anode, gadolinia-doped ceria electrolyte and $Sm_{0.5}Sr_{0.5}CoO_3$-SDC cathode displayed stable operation over 11 h test using biomass-produced synthesis gas [16]. In addition, a Ni-free Cu-CeO_2-YSZ anode has been tested in a single cell and demonstrated stable voltage at the discharging current of 200 mA cm^{-2} in the gasoline operating mode for 12 h at 700 °C. No carbon was detected after the cell test [23]. These results demonstrate the effectiveness of Cu for suppressing carbon deposition and improving performance stability of single cells.

In spite of the improved stability in hydrocarbon fuels, the electrochemical activity of the Cu anode is not sufficient for SOFC applications. The Cu anodes are also less thermally stable at high temperatures and tend to coarsen over time. Alternatively, a catalytic micro-reforming/anode bilayer design was developed and studied for applications in direct hydrocarbon-fed SOFCs [5,24–28]. In such cell configurations, hydrocarbon fuels are partially oxidized to synthesis gas in the micro-reforming outer layer. The synthesis gas then diffuses to the electrochemically active inner anode layer for electrochemical oxidation. For example, both 9.1 wt.% RuO_2-90.9 wt.% ceria and 0.5 wt.% Rh-99.5 wt.% gadolinia-doped ceria have been fabricated as the catalytic micro-reforming layer and integrated over a conventional Ni-YSZ anode [5,26,27]. In the presence of the internal micro-reforming layer, the single cell displayed the maximum power output of ≥600 mW cm^{-2} and stable performance over 200 h in both isooctane and *n*-butane fuels. However, the use of noble metals is less desirable because of their high cost. Recently, an alternative inexpensive Mo-modified Ni-Ce-Zr-based catalyst has been developed, which showed excellent partial oxidation performance toward various logistic fuels. This Ni-Mo-ceria-zirconia catalyst was fabricated into the internal micro-reforming layer and integrated with a conventional Ni-YSZ anode supported single cell [29,30]. The single cell displayed a high maximum power density of 405 mW cm^{-2} at 0.55 V under the isooctane/air feed condition at 750 °C and exhibited good stability at a current density of 500 mA cm^{-2} over the 12 h test.

In addition to the high reforming activity obtained in our previous work, the Ni-Mo-Ce-Zr-based material can efficiently conduct both electrons and oxygen ions [30,31]. Hence, the Ni-Mo-Ce-Zr-based material has the potential to be applied as the single anode layer of a SOFC to provide both high internal reforming activity and high electrochemical activity. To apply it as the single anode layer, Ni-Mo-Ce-Zr has to be sintered at high temperatures (~1400 °C) to ensure a good connectivity between grains for efficient conductions of electrons and oxygen ions. On the other hand, high temperature sintering will increase the grain size of the catalyst and reduce the available catalytic surface. Thus, further research efforts are necessary to optimize the single Ni-Mo-Ce-Zr anode layer design for SOFC applications. In this work, we fabricated an electrolyte-supported SOFC using a Mo-modified Ni-Ce-Zr single anode layer and studied its internal reforming and electrochemical performance under the isooctane/air mixture feed condition.

2. Experimental

2.1. Synthesis of NiMo oxide-ceria-zirconia

The NiMo oxide-ceria-zirconia powder was synthesized by ball-milling and impregnation methods. NiO (Sigma Aldrich) and ceria-zirconia ($Ce_{0.5}Zr_{0.5}O_2$, CZ, from Alfa) were thoroughly mixed in ethanol by ball-milling for 24 h. The mixture was dried at 80 °C and calcined at 1000 °C for 1 h in air. Molybdenum was introduced into the NiO-ceria-zirconia powder by wet impregnation. Ammonium heptamolybdate ($(NH_4)_6Mo_7O_{24}{\cdot}4H_2O$ from Sigma Aldrich) was dissolved in distilled water and slowly impregnated into the NiO-CZ powder followed by calcining at 500 °C for 1 h in air. Before reduction, the total NiO-MoO_x content in the powder was 50 wt.%, and the Mo fraction in the NiO-MoO_x system was 0 wt.%, 3 wt.% and 5 wt.% (NiO-CZ, NiO-3MoO_x-CZ, and NiO-5MoO_x-CZ), respectively. For characterization purposes, the mixed powders were reduced in hydrogen at 700 °C for 2 h, and the reduced samples are referred to as Ni-CZ, Ni-3Mo-CZ, and Ni-5Mo-CZ, respectively.

2.2. Single cell fabrication

Electrochemical performance of the Ni-Mo-CZ anodes was evaluated using an electrolyte-supported button single cell. The cell was comprised of a Ni-Mo-CZ anode, yttria-doped zirconia ($Zr_{0.98}Y_{0.08}O_{2-\delta}$, YSZ) electrolyte, $Ce_{0.8}Sm_{0.2}O_{1.9}$ buffer layer, and $La_{0.6}Sr_{0.4}Co_{0.2}Fe_{0.8}O_{3-\delta}$ cathode. To prevent the chemical reaction between the YSZ electrolyte and the $La_{0.6}Sr_{0.4}Co_{0.2}Fe_{0.8}O_{3-\delta}$ cathode, a thin $Ce_{0.8}Sm_{0.2}O_{1.9}$ buffer layer was deposited between the electrolyte and the cathode [32].

For the $Ce_{0.8}Sm_{0.2}O_{1.9}$ buffer layer fabrication, a slurry consisting of 14.1 wt.% $Ce_{0.8}Sm_{0.2}O_{1.9}$, 85.1 wt.% ethanol, and 0.8 wt.% ethyl cellulose (Sigma Aldrich) was spin-coated over the electrolyte substrate ($Zr_{0.98}Y_{0.08}O_{2-\delta}$, Fuel Cell Materials, fuelcellmaterials.com) at a rotation speed of 3000 rpm for 40 s. The deposited layer was calcined at 700 °C for 1 h in air to remove the residual organics.

The NiO-Mo-CZ layer was deposited on the opposite side of the electrolyte by screen-printing a slurry consisting of 10 wt.% anode powder mixed with 90 wt.% terpineol and then calcined at 700 °C for 1 h in air. This step was repeated three times to achieve the desired thickness of the anode layer (> 20 μm). The final anode layer was sintered at 1400 °C for 1 h in air.

The $La_{0.6}Sr_{0.4}Co_{0.2}Fe_{0.8}O_{3-\delta}$ cathode was deposited on top of the $Ce_{0.8}Sm_{0.2}O_{1.9}$ buffer layer by spin-coating. The cathode slurry was prepared by mixing 14.1 wt.% $La_{0.6}Sr_{0.4}Co_{0.2}Fe_{0.8}O_{3-\delta}$ powder (Fuel Cell Materials), 85.1 wt.% ethanol and 0.8 wt.% ethyl cellulose in a rotational ball mill for 24 h. This cathode slurry was spin-coated onto the $Ce_{0.8}Sm_{0.2}O_{1.9}$ buffer layer at 3000 rpm for 40 s, followed by calcining at 700 °C for 1 h in air. The step was repeated four times and the cathode was finally sintered at 1000 °C for 2 h in air [33]. The active surface area of the single cells is 1.00 cm^2. A schematic diagram of the electrolyte supported single cell is shown in Fig. 1.

For comparison purpose, an electrolyte-supported single cell with the conventional Ni-YSZ anode, YSZ electrolyte, $Ce_{0.8}Sm_{0.2}O_{1.9}$ buffer layer, and $La_{0.6}Sr_{0.4}Co_{0.2}Fe_{0.8}O_{3-\delta}$ cathode was fabricated. 50 wt.% NiO and 50 wt.% YSZ powder was employed to deposit the anode layer and the fabrication process is the same as that used for fabricating the Ni-Mo-CZ anode single cell.

2.3. Structural characterization

The crystal phases of the NiO-Mo-CZ and Ni-Mo-CZ samples were examined using an X-ray diffractometer (XRD, Rigaku Miniflex 600) with Cu Kα radiation at 40 kV and 15 mA. The XRD patterns were scanned in continuous mode from 20 to 80° at 1° min^{-1}.

The morphology of the Ni-Mo-CZ powders and the microstructure of the electrolyte-supported single cell were examined by scanning electron microscopy (SEM, FEI Quanta 450). Image analysis was used to estimate the average particle sizes of the powders [34].

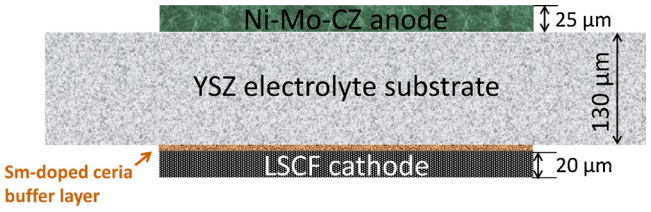

Fig. 1. Schematic diagram of the electrolyte-supported single cell.

2.4. Conductivity of Ni-Mo-CZ

The conductivity of Ni-Mo-CZ ceramics was measured by the direct current (DC) four-probe technique using an electrochemical workstation (Metrohm Autolab 302N). For the DC four-probe measurement, the NiO-Mo-CZ powders were hydraulically compressed into rectangular bar samples and sintered at 1400 °C for 4 h in air. The bar samples were then reduced at 800 °C for 2 h in hydrogen. The details of the conductivity test have been reported elsewhere [33].

2.5. Catalytic activity of Ni-Mo-CZ composite

The catalytic activity of the Ni-Mo-CZ composite for isooctane conversion to synthesis gas was evaluated under the open circuit voltage (OCV) condition during the *in-situ* button cell testing. The inlet flow rates of gases were controlled by a set of mass flow controllers (Brooks 5850E) and the composition of the exhaust gas was analyzed by gas chromatography (SRI 8610C). The isooctane conversion and H_2, CO and CH_4 yields were calculatedas follows [29]:

$$\text{Isooctane conversion} = (\text{total moles of CO, } CO_2 \text{ and } CH_4)/(8 \times \text{moles of isooctane fed}) \quad (1)$$

$$H_2 \text{ yield} = (2 \times \text{moles of } H_2)/(18 \times \text{moles of isooctane fed}) \quad (2)$$

$$\text{CO yield} = (1 \times \text{moles of CO})/(8 \times \text{moles of isooctane fed}) \quad (3)$$

$$CH_4 \text{ yield} = (1 \times \text{moles of } CH_4)/(8 \times \text{moles of isooctane fed}) \quad (4)$$

2.6. Electrochemical measurements

Electrochemical performance of the electrolyte-supported single cell was evaluated using an in-house-designed fuel cell testing system. The system consists of an electrochemical workstation (Metrohm Autolab M101), a DC electric load (BK precision 8500), mass flow controllers, and alumina cell holders. The electrolyte-supported single cell was sealed on the alumina holder by an alumina-based ceramic binder (AREMCO Products). Electrochemical cell characterization was performed initially using dry hydrogen (50 sccm) as fuel and air as the oxidant at 800 °C. Then, a mixture of isooctane and air was used as the fuel. In order to feed this fuel mixture to the anode, 100 sccm air was bubbled through liquid isooctane at room temperature. The isooctane and air molar ratio of the fuel mixture leaving the bubbler was determined to be 1:20, which is comparable with previously published data with a similar experimental setup [27]. Electrochemical impedance spectra of the single cells were collected at the OCV condition in the frequency range 0.01 Hz to 100 kHz. Cell performance was evaluated in isooctane/air at 800 °C by monitoring cell voltages at a fixed current density.

3. Results and discussion

3.1. Structural investigation

Fig. 2 shows XRD patterns from the NiO-Mo-CZ and Ni-Mo-CZ powders, respectively. In Fig. 2(a), the characteristic diffraction peaks of NiO (2θ = 43.28°) and CZ were observed for the unreduced samples (NiO-Mo-CZ). Fig. 2(b) shows the characteristic diffraction peaks for the metallic Ni phase (2θ = 44.54°) after the reduction in hydrogen. No additional peaks corresponding to the Mo phase could be identified within the sensitivity of the XRD measurement. By increasing the amount of Mo in Ni-Mo-CZ, the diffraction peaks corresponding to the Ni phase shifted towards lower 2θ values (Fig. 2(c)), indicating the formation of NiMo solid solutions. Rietveld refinement was used to estimate the lattice parameters of the NiMo alloy in the composites and the results are listed in Table 1 [35]. In general, the incorporation of Mo resulted in an expansion of the Ni lattice, which could be due to the

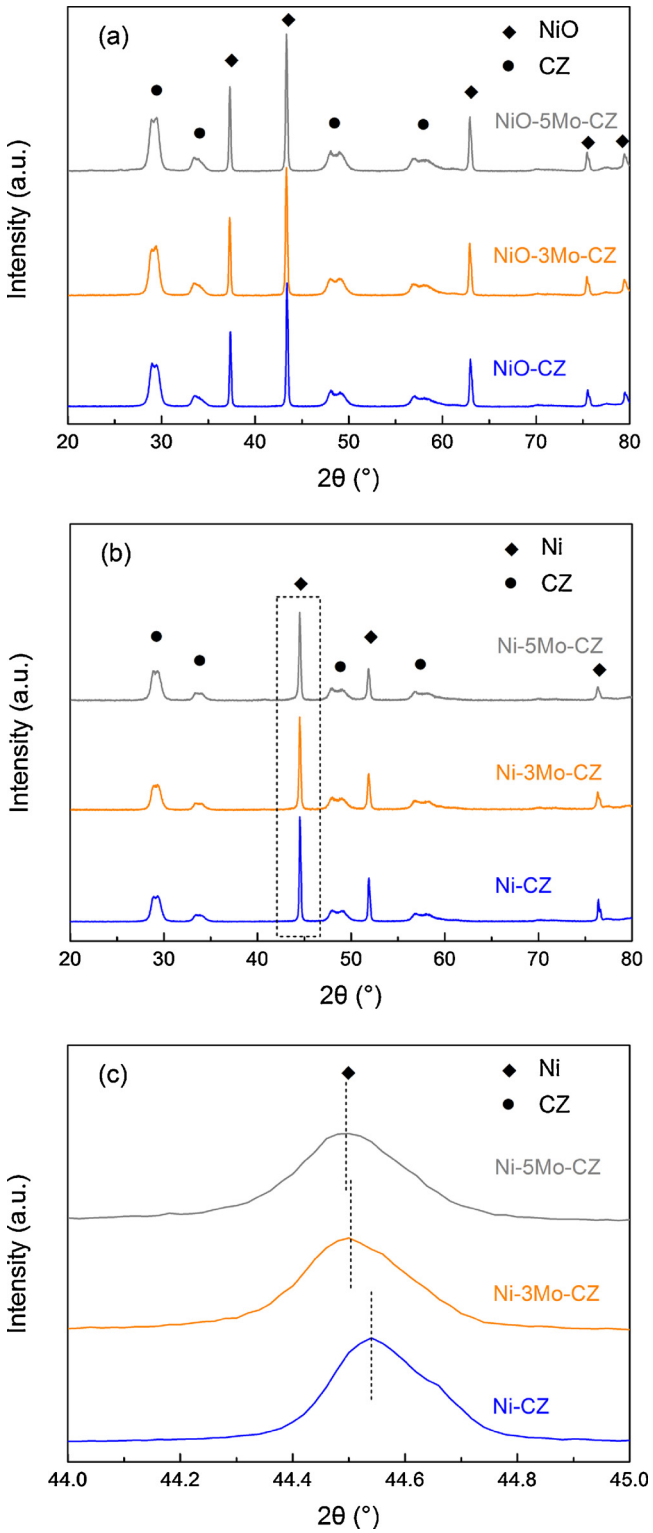

Fig. 2. XRD patterns of (a) NiO-Mo-CZ and (b) Ni-Mo-CZ powders at 2θ range of 20–80°. (c) Short range XRD data for the Ni-Mo-CZ powders.

Table 1
Lattice parameters determined from Rietveld refinement for Ni-CZ, Ni-3Mo-CZ, and Ni-5Mo-CZ powders.

Samples	Ni-CZ	Ni-3Mo-CZ	Ni-5Mo-CZ
Lattice parameter (Å)	3.5205 ± 0.0003	3.5236 ± 0.0005	3.5237 ± 0.0005

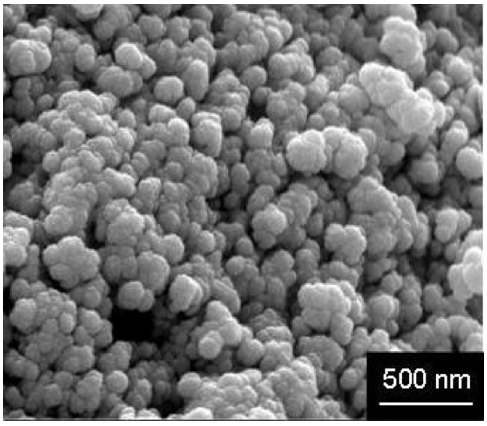

Fig. 3. SEM image of Ni-Mo-CZ powder synthesized by the wet-impregnation method.

larger size of Mo atoms (1.45 Å) compared to Ni atoms (1.35 Å) [36].

Fig. 3 shows a typical SEM image of the Ni-5Mo-CZ powder synthesized by the wet-impregnation process. The powder consists of weakly agglomerated homogeneous particles. Using image analysis, the average particle size was estimated to be 150 nm [34]. The SEM analysis revealed that the Ni-Mo-CZ powders with different molybdenum contents shared a similar morphology.

3.2. Electrical conductivity

Fig. 4 shows the electrical conductivity of the Ni-Mo-CZ composites with different amounts of Mo measured in dry hydrogen at 500–800 °C. Note that while the samples were sintered to 88%–96% of theoretical density in air, they became porous upon reduction. The final porosity was measured to be 28%–35% using the Archimedes' method [37]. The details of the porosity measurement are described in the Supplementary material. For each sample, the conductivity decreased with increasing temperature. This trend agrees with that typically shown by metallic electronic conductors, indicating the metal component dominating the overall conducting properties of the Ni-Mo-CZ composite. The result also aligns well with that obtained from conventional Ni-YSZ and Ni-samaria-doped ceria anode materials [38,39]. The conductivities of the Mo-containing samples were higher than that of the Ni-CZ sample. This result could be due to the enhanced sintering effect of the Mo. As shown in the Supplementary materials (Fig. S1), the shrinkage of the sample increased when Mo was introduced. If the Mo acts as a sintering agent,

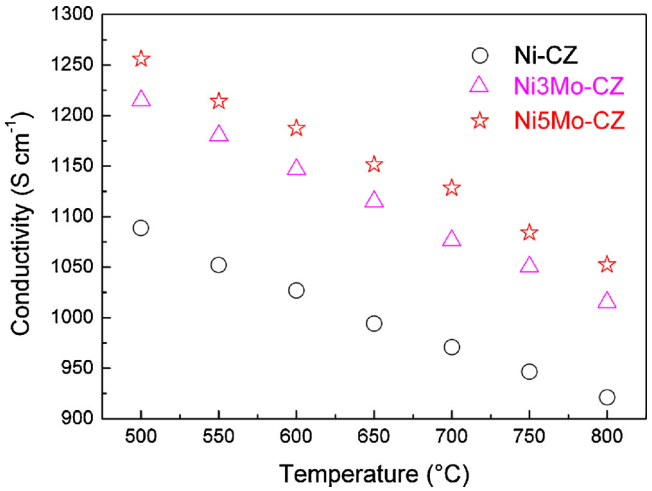

Fig. 4. Electrical conductivity of Ni-Mo-CZ in dry hydrogen at 500–800 °C for different Mo contents.

it could improve the overall connectivity between the grains in the NiO-Mo-CZ ceramics, and thus higher overall conductivity upon reduction.

3.3. Microstructure of the single cell

Fig. 5 shows cross-sectional SEM images of a cell with the Ni-5Mo-CZ anode, $La_{0.6}Sr_{0.4}Co_{0.2}Fe_{0.8}O_{3-\delta}$ cathode, $Ce_{0.8}Sm_{0.2}O_{1.9}$ buffer layer and YSZ electrolyte. Fig. 5(a) illustrates the full single cell with both electrodes. Good adhesion was obtained between the different layers. Fig. 5(b) and (c) show the electrolyte-anode and electrolyte-cathode interfaces, respectively. Both electrodes are seen to be porous with a uniform distribution of micron-sized particles and pores. The electrolyte layer is dense with no open porosity. The thicknesses of cell functional layers were determined by SEM/EDS image analysis. The thicknesses of the anode, electrolyte, buffer layer, and cathode were determined to be 20, 130, 3, and 25 μm, respectively.

3.4. Catalytic activity test

The catalytic activity of the Ni-YSZ anode, Ni-CZ anode, and Ni-5Mo-CZ anode toward partial oxidation of isooctane to synthesis gas was comparatively studied using a button cell kept at the OCV conditions at 800 °C. Fig. 6 shows the isooctane conversion and H_2, CO, and CH_4 yields for Ni-YSZ anode, Ni-CZ anode, and Ni-5Mo-CZ anode, respectively. As is well known, isooctane can be thermally pyrolyzed at 800 °C even without the presence of catalysts, and the cracked hydrocarbon fragments (such as CH_4, C_6H_6, C_2H_2, and C_2H_4) could be partially oxidized by the oxygen in the gas mixture. To study the role of gas-phase oxidative reforming of isooctane without the anode catalyst, we performed a blank test using only the electrolyte substrate (without the anode layer) under the same measurement condition. Fig. 6(a) shows the isooctane conversion and H_2, CO, and CH_4 yields obtained from the cell without the anode layer (a blank cell). The oxidative pyrolysis of isooctane at 800 °C presented an isooctane conversion of 37%, as well as low H_2 yield (5.7%) and low CO yield (4.0%). As shown in Fig. 6(b), with the Ni-YSZ anode, the initial isooctane conversion was increased to ~50%, and the H_2 and CO yields were enhanced to ~20%. Despite the improved initial performance, the reforming activity of Ni-YSZ anode significantly decreased in 1000 min. After the reforming test, a large amount of carbon species could be seen on the anode surface. The carbon was confirmed by the XRD measurement on the anode (shown in Fig. S5 in the Supplementary material). Hence, the Ni-YSZ single cell cannot be operated under the isooctane/air mixture at 800 °C.

The ceria-zirconia-based materials show a high oxygen storage capacity, which could be utilized to oxidize the carbon species deposited on the Ni-containing anode before they form coke [40]. Based on this consideration, we replaced the Ni-YSZ with a Ni-CZ in the anode. Fig. 6(c) shows the isooctane conversion and H_2, CO, and CH_4 yields obtained from the cell using Ni-CZ anode. The Ni-CZ anode presented similar initial reforming activity compared with that of Ni-YSZ, while the stability was greatly enhanced. After the reforming test, no visible carbon could be identified in the anode. This result suggests that the CZ processes a higher coking resistance than the YSZ for catalytic partial oxidation of isooctane in the cell.

Our previous research indicated that the nano-sized Ni-CZ catalysts in the pack-bed reactor showed high isooctane conversion of > 75%, and the addition of Mo in the Ni-CZ could further enhance the reforming activity, where isooctane conversion was ~95% and the H_2 and CO yields were 73% and 80%, respectively [30]. Thus, we applied the Ni-5Mo-CZ as the anode of the single cell and studied its reforming performance under the OCV condition as well. Fig. 6(d) shows the reforming performance of the Ni-5Mo-CZ anode. The Ni-5Mo-CZ anode presented stable isooctane conversion of 50% and the H_2, CO and CH_4 yields were ~20%. When we compare the reforming performances of two catalysts (Ni-CZ and Ni-5Mo-CZ) from both the pack-bed reactor

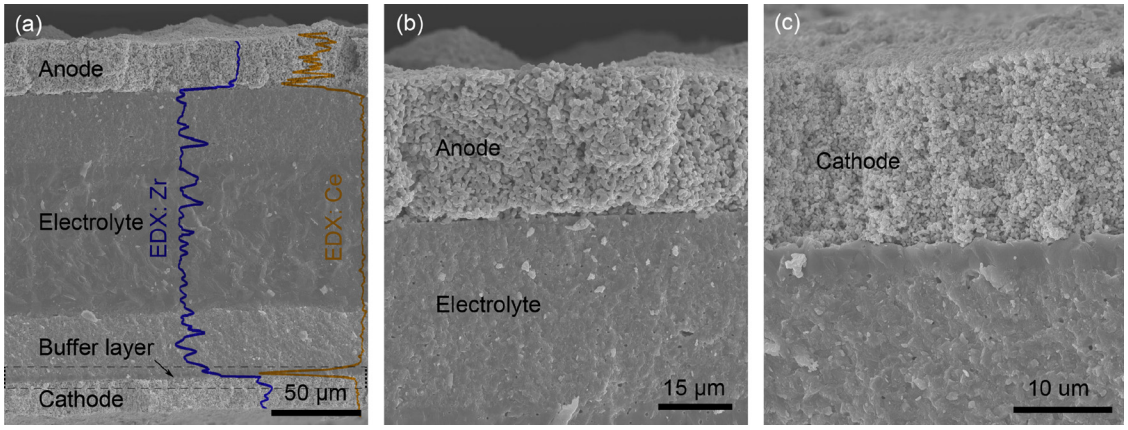

Fig. 5. SEM cross-section images of the single cell: (a) low magnification image, and (b) and (c) higher magnification images.

and SOFC at the OCV modes, we made two important observations: (1) both catalysts show much higher reforming performances from the pack-bed reactor mode than the SOFC at the OCV mode; and (2) the reforming performances of both Ni-CZ and Ni-Mo-CZ from the SOFC at the OCV mode are very similar despite the fact that the reforming performance of Ni-Mo-CZ is much higher than that of Ni-CZ from the pack-bed reactor mode.

The lower reforming activities for the isooctane partial oxidation from our single cells at the OCV condition compared to their reforming activities from the pack-bed reactors are likely due to the larger Ni-CZ and Ni-5Mo-CZ grains in the sintered composite. In the previous study, the nano-sized Ni-CZ and Ni-Mo-CZ powder catalyst was employed in the conventional pack-bed reforming reactor and had a specific surface area $> 100\,m^2\,g^{-1}$. The high specific surface area is beneficial for increasing the overall non-electrochemical reforming activity. However, the cells employing the Ni-CZ and Ni-Mo-CZ anodes in this study were

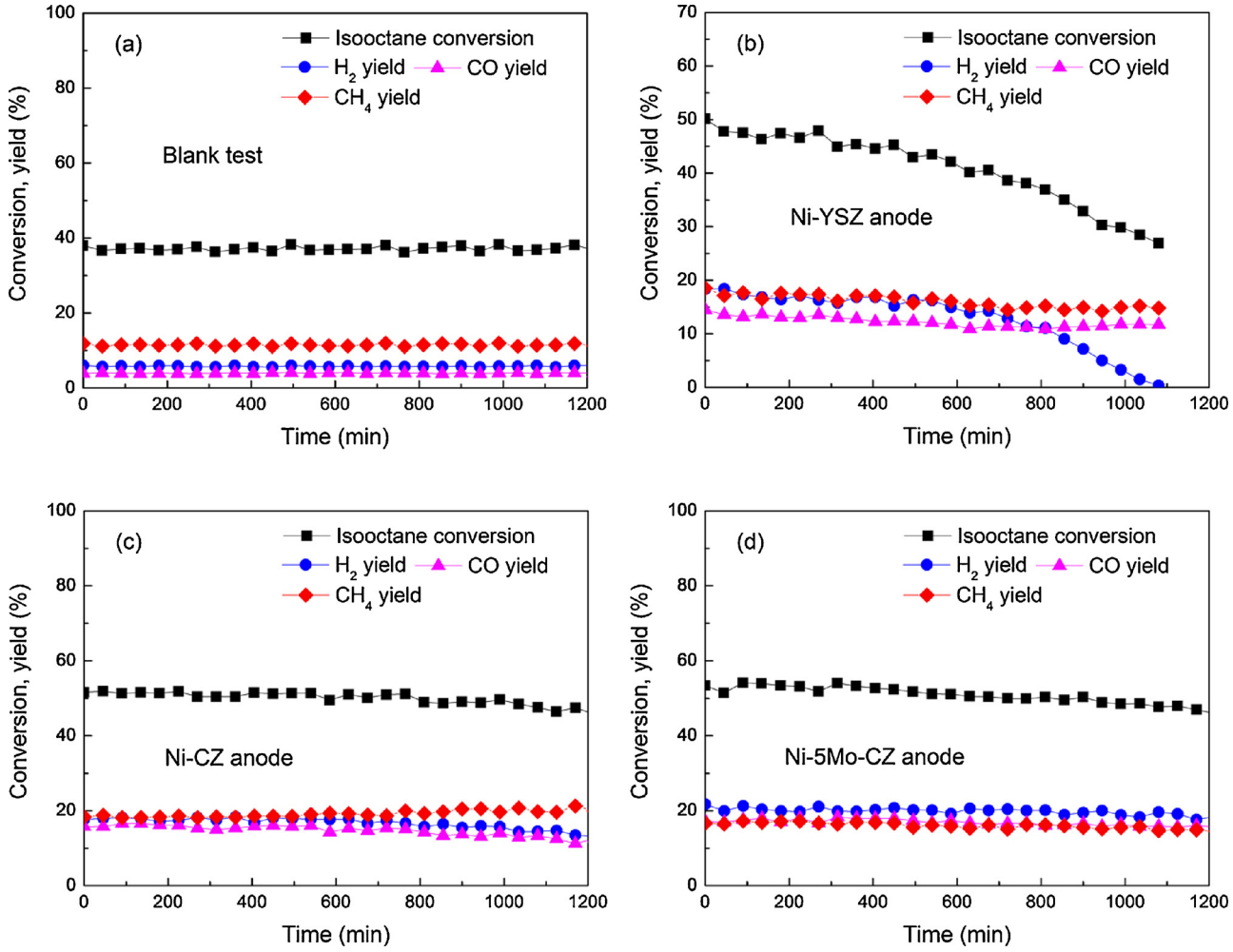

Fig. 6. Gas compositions from the anode exhaust of the single cells at the OCV condition at 800 °C: (a) blank test (no electrode, only YSZ substrate), (b) conventional Ni-YSZ anode, (c) Ni-CZ anode, and (d) Ni-5Mo-CZ anode.

sintered at 1400 °C to ensure good connectivity in the anodes for enhancing electrochemical reactions, which resulted in a much lower specific surface area (< 5 $m^2 g^{-1}$) than the pack-bed catalyst [8,41]. Consequently, the reforming activities of both Ni-CZ and Ni-Mo-CZ reduced significantly from the single cells at the OCV condition. In addition, in our previous pack-bed reactor tests, the gases were fed through the catalyst pack-bed and the long residence time allowed for high fuel conversions [30]. In our fuel cell test geometry (Supplementary material, Fig. S2), the residence time is expected to be much lower because some of the input gas could bypass the anode layer without penetrating through the catalyst layer. This difference in the gas circulation mode could lead to the lower reforming performances from the anode catalyst of the single cells at the OCV condition. As a result of both the low specific surface area of the anode and low residence time of the reactive gas associated with the single cell design and the test setup, the reforming activity difference between the Ni-CZ and Ni-Mo-CZ anodes of the single cells at the OCV condition cannot be observed in the present study.

3.5. Electrochemical performance

Fig. 7(a) shows the voltage and power density of single cells as a function of current density measured at 800 °C using dry hydrogen fuel. The OCV values of cells tested were above 1.10 V, indicating good sealing in the experimental setup [42]. The single cell with the Ni-CZ anode exhibited a maximum power density (MPD) of 260 mW cm^{-2}. When adding 5 wt.% Mo into the Ni-CZ anode, the MPD increased to 420 mW cm^{-2}. The enhanced maximum power output suggested the positive effect of Mo on the electrochemical performance of the anode. In addition, the MPD of the Ni-5Mo-CZ anode single cell was comparable with the conventional Ni-YSZ anode single cell shown in the Supplementary material (Fig. S3 in the Supplementary material) [43].

Fig. 7(b) shows Nyquist plots of the single cell under the OCV condition at 800 °C using dry hydrogen fuel. The electrochemical impedance spectra were fitted by the $LR_{ohm}(R_HQ_H)(R_MQ_M)(R_LQ_L)$ equivalent circuit model (shown in the insert of Fig. 7(b)) using the Zview software [44]. The fitting was performed by applying a set of impedance data in the full frequency range of 0.01 Hz to 100 kHz. The inductance circuit element L represents the inductive impedance response, which originates from the connecting wires and the measurement devices. The R_{ohm} is the ohmic resistance of the single cell. The $(R_HQ_H)(R_MQ_M)(R_LQ_L)$ components denote a sum of the electrode processes from both the anode and the cathode, where R is the resistance and Q is the constant phase element. The subscripts H, M, and L represent the electrochemical processes from high frequency, middle frequency, and low frequency arcs, respectively. As the cathode condition was kept constant in this experiment, the variation of the component values can be ascribed to the anode layer. The electrode resistance (R_p) of the single cell is the sum of R_H, R_M and R_L [45–48].

Table 2
Ohmic and electrodic losses of cells with different anodes at 800 °C.

Anode	Ni-CZ	Ni-5Mo-CZ	Ni-CZ	Ni-5Mo-CZ
	Hydrogen		Isooctane/air	
R_{ohm} (Ω cm^2)	0.30	0.28	0.70	0.65
R_p (Ω cm^2)	6.98	3.81	28.97	19.28

Table 2 lists ohmic and polarization resistances of the single cells obtained by fitting the impedance spectra. All cells exhibited similar ohmic resistances (0.28-0.31 Ω cm^2) in the dry hydrogen fuel, which is likely due to the YSZ electrolyte resistance. Since identical YSZ substrates were used in all cells, similar ohmic losses were measured. When adding 5 wt.% Mo into the Ni-CZ anode, the cell losses due to the electrode reactions (R_p) decreased from 6.98 to 3.81 Ω cm^2, indicating the reduction of anode resistance: the cathodes were unchanged. The reduced anodic losses could be explained by the Mo promoting effect. As shown in Fig. S1 in the Supplementary material, the addition of Mo is found to facilitate the sintering of the anode at 1400 °C. This would improve the connection between the grains in the anode and increase the conductivity as shown in Fig. 4, benefiting the transport of electrons and oxygen ions for the fuel oxidation in the anode. Additionally, as predicted by the DFT calculations, the hydrogen binding energy on Ni increases when the Mo is introduced to form a NiMo solid solution [49]. The increased hydrogen binding energy could enhance hydrogen adsorption and dissociation processes and reduce the resistance associated with the anodic reactions. Due to the effects of Mo on conductivity and hydrogen binding energy, the R_p of the single cell using Ni-5Mo-CZ was reduced by 45% compared with that of the Ni-CZ anode cell. Moreover, it displayed comparable electrochemical performance to the conventional Ni-YSZ anode single cell in hydrogen fuel (Fig. S3 in the Supplementary material).

Fig. 8(a) shows current-voltage curves of single cells measured in the isooctane/air mode at 800 °C. The cells with the Ni-CZ anode displayed a low MPD of 70 mW cm^{-2} indicative of rather poor anode activity. With the introduction of 5% Mo to the Ni-CZ anode, the MPD tripled to 212 mW cm^{-2}. The significantly improved electrochemical performance illustrates the effectiveness of the Ni-5Mo-CZ anode for the internal reforming of SOFC operating with the isooctane fuel.

Fig. 8(b) shows the Nyquist plots of the single cells collected under the OCV condition. The resistances determined by fitting the data are listed in Table 2 as well. All cells displayed similar ohmic losses, 0.65-0.70 Ω cm^2, that were somewhat higher than those measured in dry

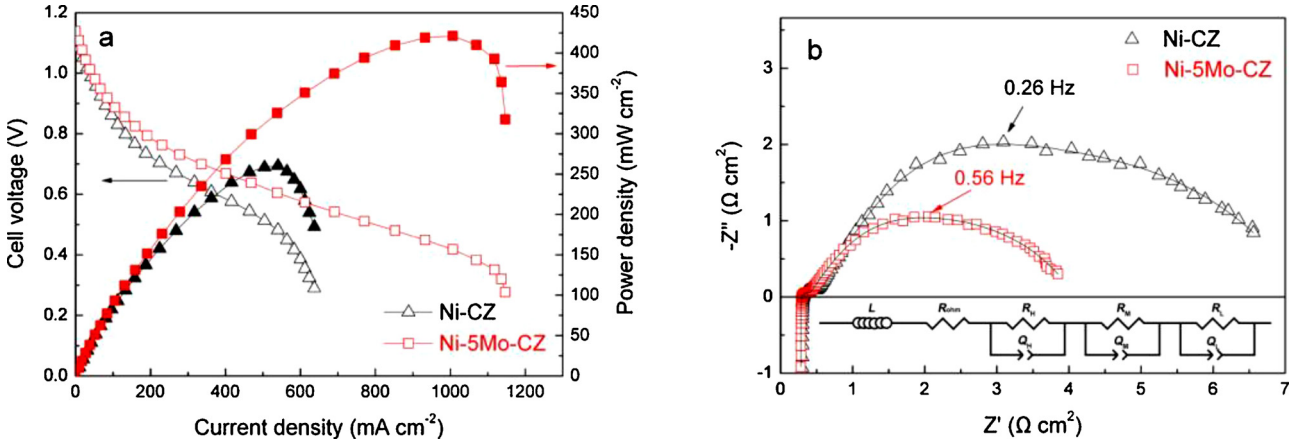

Fig. 7. (a) Current-voltage and power density curves of the single cells with different anodes in dry hydrogen at 800 °C, and (b) Nyquist plots of the single cells under the OCV condition at 800 °C.

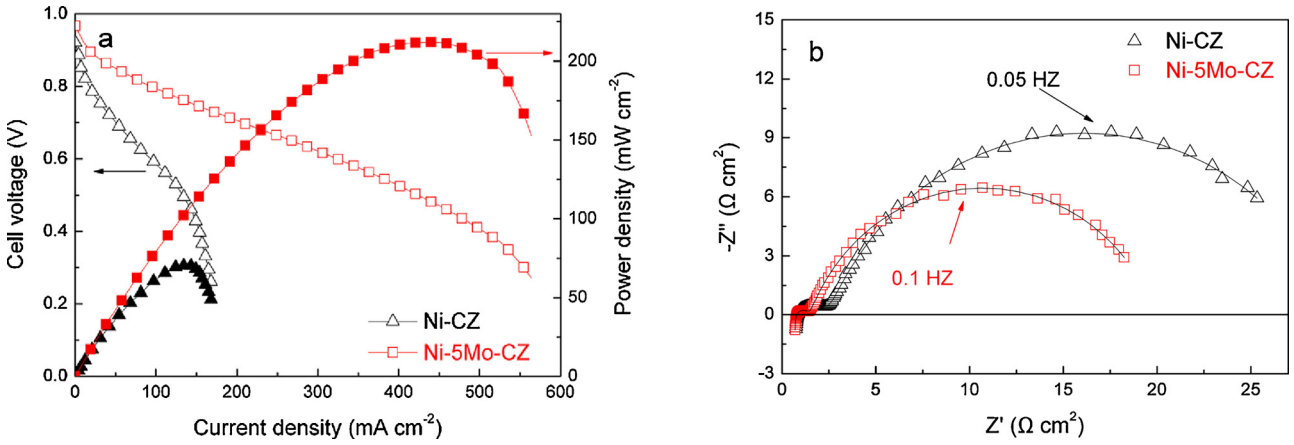

Fig. 8. (a) Current-voltage and power density curves of the single cells with different anodes in the isooctane/air mode at 800 °C, and (b) Nyquist plots of the single cells under the OCV condition at 800 °C.

hydrogen fuel. The electrodic losses in all cells were also higher compared to those measured in dry hydrogen. It is unlikely that isooctane was electrochemically oxidized without converting it first into synthesis gas via the fuel reforming reactions. Thus, the higher R_p in the isooctane/air operation mode compared to that in the dry hydrogen mode is likely due to the lower amount of the active fuels (H_2 and CO) produced via the isooctane partial oxidation. When the 5 wt.% Mo was introduced to the Ni-CZ anode, the R_p was reduced by 33.4% in the isooctane/air operation mode (See Fig. 8(b) and Table 2). As the Ni-CZ and Ni-5Mo-CZ anodes exhibited comparable internal reforming activities under the single cell condition as shown in Fig. 6, the reduced R_p value indicates the higher intrinsic electrochemical activity of the Ni-5Mo-CZ anode for the electrochemical oxidation of the synthesis gas, which was in agreement with the data obtained in the dry hydrogen fuel. As a result, the single cell with the Ni-5Mo-CZ anode presented improved MPD compared to that of the Ni-CZ anode single cell in the isooctane/air operation mode.

Fig. 9 shows the performance of cells with Ni-YSZ, Ni-CZ and Ni-5Mo-CZ anodes at 800 °C in the isooctane/air mode at current densities of 60, 80, and 280 mA cm^{-2}, respectively. For the single cell with the conventional Ni-YSZ anode, the voltage rapidly dropped at a rate of 119 mV h^{-1} and the cell died in less than 5 h after exposure to isooctane. When employing the Ni-CZ anode, the cell displayed improved performance stability with a slower deactivation rate of 5 mV h^{-1} during its first 25 h test, while the voltage dropped faster in the next 5 h. With the Ni-5Mo-CZ anode, the cell voltage did not change over the 30 h test.

Following termination of all the tests, each anode layer was carefully separated from the electrolyte and the anode was analyzed by XRD (shown in Supplementary materials as Fig. S5). The quantity of deposited carbon was estimated by XRD Whole Pattern Fitting and Rietveld Refinement methods. The amount of carbon was determined to be 18.4 wt.% in the Ni-YSZ anode, 11.6 wt.% in the Ni-CZ, and 5.8 wt.% in the Ni-5Mo-CZ anode. Based on this result, we can speculate that the severe carbon deposition is the main reason for the fast degradation of Ni-YSZ anode single cell under the isooctane/air operation mode. The application of CZ in the anode improves the reforming stability as shown in Fig. 6(c) due to its higher oxygen storage capacity. Consequently, the Ni-CZ anode single cell presented the enhanced performance stability and reduced carbon deposition compared to that of Ni-YSZ anode single cell. With the additional Mo into Ni-CZ, the Ni-5Mo-CZ anode illustrated an improved electrochemical performance as evidenced by its higher current density of 280 mA cm^{-2} at the cell voltage of ~0.65 V.

According to Fig. 6, the reforming data between Ni-CZ and Ni-5Mo-CZ anodes at OCV condition are comparable. Unlike their reforming performance data, Ni-5Mo-CZ anode single cell shows the improved fuel cell stability at the constant load condition by reducing the carbon deposition compared to that of Ni-CZ anode single cell in Fig. 9. One of explanations for this enhanced stability of Ni-5Mo-CZ anode single cell is that it produced the higher current density at the cell voltage of ~0.65 V. At this increased current density, the cell can introduce the higher concentration of lattice oxygen to its anode that can mitigate the carbon deposition.

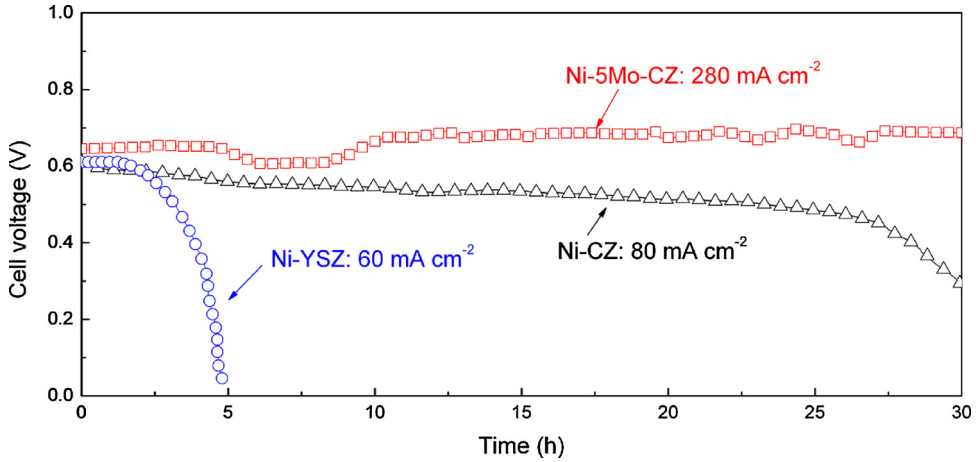

Fig. 9. Performance test of SOFCs with Ni-YSZ, Ni-CZ and Ni-5Mo-CZ anodes, respectively, at 800 °C operated on isooctane/air.

4. Conclusions

A multi-functional Ni-5Mo-CZ composite was developed and successfully tested as the single-layer anode for a SOFC operated using the isooctane/air mixture. Catalytic reforming and electrochemical performance of Ni-5Mo-CZ was investigated on the electrolyte-supported cell consisting of a Ni-5Mo-CZ anode, YSZ electrolyte and $La_{0.6}Sr_{0.4}Co_{0.2}Fe_{0.8}O_{3-\delta}$ cathode. The addition of Mo in Ni-CZ was found to facilitate sintering of the anode, which leads to the decrease of the electrode resistance of the single cell. Consequently, the single cell with the Ni-5Mo-CZ anode displayed the high MPD of 420 mW cm^{-2} in dry hydrogen fuel at 800 °C, which is comparable with that of a conventional Ni-YSZ anode single cell. When operating the cell using the isooctane/air mixture, the unique oxygen storage capacity of CZ component could improve its reforming stability towards the catalytic partial oxidation of isooctane. As a result, the cell with the Ni-5Mo-CZ anode operated for 30 h using the isooctane/air mixture without any degradation. In summary, the significantly improved performance of the Ni-5Mo-CZ anode of the single cell in the isooctane/air operation mode could be attributed to (1) the enhanced reforming function of its CZ component for mitigating the carbon deposition and (2) the sintering promoting effect of Mo for improving its conductivity and electrochemical activity. The results obtained demonstrate the potential of the single Ni-5Mo-CZ anode layer for the use in SOFCs operated on complex liquid isooctane fuels.

Acknowledgments

Xiaoxue Hou and Kai Zhao contributed equally to this work. This work was supported financially by the Office of Naval Research (Grant No. N00014-15-1-2416).

Appendix A. Supplementary data

Supplementary material related to this article can be found, in the online version, at doi:https://doi.org/10.1016/j.apcatb.2018.09.095.

References

[1] A.B. Stambouli, E. Traversa, Solid oxide fuel cells (SOFCs): a review of an environmentally clean and efficient source of energy, Renew. Sustain. Energy Rev. 6 (2002) 433–455.
[2] M. Cimenti, J. Hill, Direct utilization of liquid fuels in SOFC for portable applications: challenges for the selection of alternative anodes, Energies 2 (2009) 377–410.
[3] P. Leone, A. Lanzini, G.A. Ortigoza-Villalba, R. Borchiellini, Operation of a solid oxide fuel cell under direct internal reforming of liquid fuels, Chem. Eng. J. 191 (2012) 349–355.
[4] T. Quang-Tuyen, Y. Shiratori, K. Sasaki, Feasibility of palm-biodiesel fuel for a direct internal reforming solid oxide fuel cell, Int. J. Energy Res. 37 (2012) 609–616.
[5] Z. Zhan, S.A. Barnett, An octane-fueled solid oxide fuel cell, Science 308 (2005) 844–847.
[6] J. Vancoillie, J. Demuynck, L. Sileghem, M. Van De Ginste, S. Verhelst, Comparison of the renewable transportation fuels, hydrogen and methanol formed from hydrogen, with gasoline - engine efficiency study, Int. J. Hydrogen Energy 37 (2012) 9914–9924.
[7] A. De Sa, S. Al Zubaidy, Gas turbine performance at varying ambient temperature, Appl. Therm. Eng. 31 (2011) 2735–2739.
[8] B. Shri Prakash, S. Senthil Kumar, S.T. Aruna, Properties and development of Ni/YSZ as an anode material in solid oxide fuel cell: a review, Renew. Sustain. Energy Rev. 36 (2014) 149–179.
[9] S.P.S. Shaikh, A. Muchtar, M.R. Somalu, A review on the selection of anode materials for solid-oxide fuel cells, Renew. Sustain. Energy Rev. 51 (2015) 1–8.
[10] T. Mahata, S.R. Nair, R.K. Lenka, P.K. Sinha, Fabrication of Ni-YSZ anode supported tubular SOFC through iso-pressing and co-firing route, Int. J. Hydrogen Energy 37 (2012) 3874–3882.
[11] B. Novosel, M. Marinšek, J. Maček, Deactivation of Ni-YSZ material in dry methane and oxidation of various forms of deposited carbon, J. Fuel Cell Sci. Technol. 9 (2012) 061003-061003-061007.
[12] M.A. Buccheri, A. Singh, J.M. Hill, Anode- versus electrolyte-supported Ni-YSZ/YSZ/Pt SOFCs: effect of cell design on OCV, performance and carbon formation for the direct utilization of dry methane, J. Power Sources 196 (2011) 968–976.
[13] D. Yoon, A. Manthiram, Ni-M (M = Sn and Sb) intermetallic-based catalytic functional layer as a built-in safeguard for hydrocarbon-fueled solid oxide fuel cells, J. Mater. Chem. A 3 (2015) 21824–21831.
[14] B. Huang, S.R. Wang, R.Z. Liu, T.L. Wen, Preparation and performance characterization of the Fe-Ni/ScSZ cermet anode for oxidation of ethanol fuel in SOFCs, J. Power Sources 167 (2007) 288–294.
[15] C.K. Cho, B.H. Choi, K.T. Lee, Electrochemical performance of $Ni_{1-x}Fe_x$-$Ce_{0.8}Gd_{0.2}O_{1.9}$ cermet anodes for solid oxide fuel cells using hydrocarbon fuel, Ceram. Int. 39 (2013) 389–394.
[16] Z. Xie, C. Xia, M. Zhang, W. Zhu, H. Wang, $Ni_{1-x}Cu_x$ alloy-based anodes for low-temperature solid oxide fuel cells with biomass-produced gas as fuel, J. Power Sources 161 (2006) 1056–1061.
[17] K. Zhao, K.S. Lee, M. Chen, B.H. Kim, Q. Xu, B.G. Ahn, Electrochemical performance of a copper-impregnated Ni-$Ce_{0.8}Sm_{0.2}O_{1.9}$ anode running on methane, Int. J. Hydrogen Energy 38 (2013) 3750–3756.
[18] M. Miyake, S. Matsumoto, M. Iwami, S. Nishimoto, Y. Kameshima, Electrochemical performances of $Ni_{1-x}Cu_x$/SDC cermet anodes for intermediate-temperature SOFCs using syngas fuel, Int. J. Hydrogen Energy 41 (2016) 13625–13631.
[19] E.W. Park, H. Moon, M.S. Park, S.H. Hyun, Fabrication and characterization of Cu-Ni-YSZ SOFC anodes for direct use of methane via Cu-electroplating, Int. J. Hydrogen Energy 34 (2009) 5537–5545.
[20] C.M. Grgicak, M.M. Pakulska, J.S. O'Brien, J.B. Giorgi, Synergistic effects of $Ni_{1-x}Co_x$-YSZ and $Ni_{1-x}Cu_x$-YSZ alloyed cermet SOFC anodes for oxidation of hydrogen and methane fuels containing H_2S, J. Power Sources 183 (2008) 26–33.
[21] O.A. Marina, C.A. Coyle, M.H. Engelhard, L.R. Pederson, Mitigation of sulfur poisoning of Ni/Zirconia SOFC anodes by antimony and tin, J. Electrochem. Soc. 158 (2011) B424–B429.
[22] W. An, X.C. Zeng, C.H. Turner, First-principles study of methane dehydrogenation on a bimetallic Cu/Ni (111) surface, J. Chem. Phys. 131 (2009) 174702–174713.
[23] R.J. Gorte, H. Kim, J.M. Vohs, Novel SOFC anodes for the direct electrochemical oxidation of hydrocarbon, J. Power Sources 106 (2002) 10–15.
[24] S. McIntosh, J.M. Vohs, R.J. Gorte, Effect of precious-metal dopants on SOFC anodes for direct utilization of hydrocarbons, Electrochem. Solid-State Lett. 6 (2003) A240–A243.
[25] M.R. Pillai, D.M. Bierschenk, S.A. Barnett, Electrochemical partial oxidation of methane in solid oxide fuel cells: effect of anode reforming activity, Catal. Lett. 121 (2008) 19–23.
[26] G. Bae, J. Bae, P. Kim-Lohsoontorn, J. Jeong, Performance of SOFC coupled with n-C_4H_{10} autothermal reformer: carbon deposition and development of anode structure, Int. J. Hydrogen Energy 35 (2010) 12346–12358.
[27] Z. Zhan, S.A. Barnett, Solid oxide fuel cells operated by internal partial oxidation reforming of iso-octane, J. Power Sources 155 (2006) 353–357.
[28] K. Zhao, B.H. Kim, Y. Du, Q. Xu, B.G. Ahn, Ceria catalyst for inert-substrate-supported tubular solid oxide fuel cells running on methane fuel, J. Power Sources 314 (2016) 10–17.
[29] K. Zhao, X. Hou, Q. Bkour, M.G. Norton, S. Ha, NiMo-ceria-zirconia catalytic reforming layer for solid oxide fuel cells running on a gasoline surrogate, Appl. Catal. B: Environ. 224 (2018) 500–507.
[30] Q. Bkour, K. Zhao, L. Scudiero, D.J. Han, C.W. Yoon, O.G. Marin-Flores, M.G. Norton, S. Ha, Synthesis and performance of ceria-zirconia supported Ni-Mo nanoparticles for partial oxidation of isooctane, Appl. Catal. B: Environ. 212 (2017) 97–105.
[31] D. Xu, Q. Wang, Z. Lu, Z. Liu, G. Zhang, W. Su, High-pressure synthesis and properties of CeO_2-ZrO_2 solid solution, Chin. Sci. Bull. 46 (2001) 801–805.
[32] K. Zhao, B.H. Kim, Q. Xu, B.G. Ahn, Fabrication and characterization of inert-substrate-supported tubular single cells by dip-coating process, J. Power Sources 245 (2014) 671–677.
[33] K. Zhao, Y. Du, Calcium-doped ceria materials for anode of solid oxide fuel cells running on methane fuel, J. Power Sources 347 (2017) 79–85.
[34] J.H. Lee, H. Moon, H.W. Lee, J. Kim, J.D. Kim, K.H. Yoon, Quantitative analysis of microstructure and its related electrical property of SOFC anode, Ni-YSZ cermet, Solid State Ionics 148 (2002) 15–26.
[35] G. Kim, S. Wang, A.J. Jacobson, L. Reimus, P. Brodersen, C.A. Mims, Rapid oxygen ion diffusion and surface exchange kinetics in $PrBaCo_2O_{5+x}$ with a perovskite related structure and ordered A cations, J. Mater. Chem. 17 (2007) 2500–2505.
[36] J.C. Slater, Atomic radii in crystals, J. Chem. Phys. 41 (1964) 3199–3204.
[37] Y.B.P. Kwan, J.R. Alcock, The impact of water impregnation method on the accuracy of open porosity measurements, J. Mater. Sci. 37 (2002) 2557–2561.
[38] T. Talebi, M.H. Sarrafi, M. Haji, B. Raissi, A. Maghsoudipour, Investigation on microstructures of NiO-YSZ composite and Ni-YSZ cermet for SOFCs, Int. J. Hydrogen Energy 35 (2010) 9440–9447.
[39] Y. Yin, W. Zhu, C. Xia, G. Meng, Gel-cast NiO-SDC composites as anodes for solid oxide fuel cells, J. Power Sources 132 (2004) 36–41.
[40] E.E. Iojoiu, M.E. Domine, T. Davidian, N. Guilhaume, C. Mirodatos, Hydrogen production by sequential cracking of biomass-derived pyrolysis oil over noble metal catalysts supported on ceria-zirconia, Appl. Catal. A: Gen. 323 (2007) 147–161.
[41] Y. Guan, Y. Gong, W. Li, J. Gelb, L. Zhang, G. Liu, X. Zhang, X. Song, C. Xia, Y. Xiong, H. Wang, Z. Wu, Y. Tian, Quantitative analysis of micro structural and conductivity evolution of Ni-YSZ anodes during thermal cycling based on nano-computed tomography, J. Power Sources 196 (2011) 10601–10605.
[42] M. Henke, J. Kallo, K.A. Friedrich, W.G. Bessler, Influence of pressurisation on SOFC performance and durability: a theoretical study, Fuel Cells 11 (2011) 581–591.
[43] J.H. Koh, Y.S. Yoo, J.W. Park, H.C. Lim, Carbon deposition and cell performance of Ni-YSZ anode support SOFC with methane fuel, Solid State Ionics 149 (2002) 157–166.
[44] R. Campana, R.I. Merino, A. Larrea, I. Villarreal, V.M. Orera, Fabrication, electrochemical characterization and thermal cycling of anode supported microtubular solid oxide fuel cells, J. Power Sources 192 (2009) 120–125.
[45] A. Leonide, V. Sonn, A. Weber, E. Ivers-Tiffée, Evaluation and modeling of the cell

resistance in anode-supported solid oxide fuel cells, J. Electrochem. Soc. 155 (2008) B36–B41.
[46] X. Zhou, K. Sun, J. Gao, S. Le, N. Zhang, P. Wang, Microstructure and electrochemical characterization of solid oxide fuel cells fabricated by co-tape casting, J. Power Sources 191 (2009) 528–533.
[47] E. Brightman, D.G. Ivey, D.J.L. Brett, N.P. Brandon, The effect of current density on H_2S-poisoning of nickel-based solid oxide fuel cell anodes, J. Power Sources 196 (2011) 7182–7187.
[48] M.J. Escudero, A. Aguadero, J.A. Alonso, L. Daza, A kinetic study of oxygen reduction reaction on La_2NiO_4 cathodes by means of impedance spectroscopy, J. Electroanal. Chem. 611 (2007) 107–116.
[49] W. An, D. Gatewood, B. Dunlap, C.H. Turner, Catalytic activity of bimetallic nickel alloys for solid-oxide fuel cell anode reactions from density-functional theory, J. Power Sources 196 (2011) 4724–4728.